

Simulation of thermos-solutal convection induced macrosegregation in a Sn-10%Pb alloy benchmark during columnar solidification

This content has been downloaded from IOPscience. Please scroll down to see the full text.

2016 IOP Conf. Ser.: Mater. Sci. Eng. 119 012004

(<http://iopscience.iop.org/1757-899X/119/1/012004>)

View [the table of contents for this issue](#), or go to the [journal homepage](#) for more

Download details:

IP Address: 193.170.16.107

This content was downloaded on 07/06/2016 at 15:45

Please note that [terms and conditions apply](#).

Simulation of thermos-solutal convection induced macrosegregation in a Sn-10%Pb alloy benchmark during columnar solidification

Y Zheng¹, M Wu^{1,2}, A Kharicha^{1,2}, A Ludwig¹

¹Chair of Modelling and Simulation of Metallurgical Processes, Montanuniversitaet Leoben, Austria

²Christian Doppler Lab for Advanced Simulation of Solidification and Melting, Montanuniversitaet Leoben, Austria

E-mail: menghuai.wu@unileoben.ac.at

Abstract: In order to investigate the effect of thermo-solutal convection on the formation of macrosegregation during columnar solidification, simulations with a liquid-columnar two phase model were carried out on a 2D rectangular benchmark of Sn-10%Pb alloy. The solidification direction in the benchmark is unidirectional: (1) downwards from top to bottom or (2) upwards from bottom to top. Thermal expansion coefficient, solutal expansion coefficient and liquid diffusion coefficient of the melt are found to be key factors influencing the final macrosegregation. The segregation range and distribution are also strongly influenced by the benchmark configurations, e.g. the solidifying direction (upwards or downwards) and boundary conditions, et al. The global macrosegregation range increases with the velocity magnitude of the melt during the process of solidification.

1 Introduction

Macrosegregation is the inhomogeneous solute distribution at the scale of a casting and it is very sensitive to thermal-solutal convection [1]. It is important to understand the macrosegregation, and be able to model and control it because macrosegregation is usually detrimental for castings. Macrosegregation is mainly due to a combination of microsegregation and relative motion between liquid phase and solid phase [2-5]. The relative motion during the solidification is induced by different flow phenomena, for example, equiaxed sedimentation, thermo-solutal convection or feeding flow. In this study it is dedicated to illustrate the delicate mechanism of macrosegregation during solidification with the presence of thermal-solutal convection. This is also an important topic in the annual solidification course in Swiss Federal Institute of Technology of Lausanne (EPFL) [4, 6]. There are lots of works carried out on lateral solidification benchmark [7-11] while the investigation on the vertical-directional solidification is not sufficient. In order to investigate the effect of thermo-solutal convection on the formation of macrosegregation during vertical-unidirectional solidification, a series of simulations with a liquid-columnar two phase model were carried out on 2D rectangular benchmark of Sn-10%Pb alloy. The aim of this paper is to explore the effect of thermo-solutal convection on macrosegregation in detail.

2. Numerical model and simulation settings

Details of the two-phase columnar solidification model are described by Wu and Ludwig [12, 13]. The main assumptions are:



- a) The two phases in the model are the liquid melt and the solidifying columnar dendrite trunks. The morphology of the columnar dendrite trunks is approximated by step-wise growing cylinders positioned in a staggered arrangement with constant primary dendritic arm spacing, λ_1 .
- b) The columnar trunks grow from the casting surface when constitutional undercooling exists and the columnar tip front is tracked explicitly.
- c) The liquid-to-solid mass transfer (solidification/melting) rate, M_{fs} , is calculated as a function of the growth velocity of the columnar trunks, v_{R_c} , which is governed by diffusion of the solute in the interdendritic melt surrounding each cylindrical trunk.
- d) Thermodynamic equilibrium is assumed at the liquid-solid interface. The concentration difference ($c_\ell^* - c_\ell$) is the driving force for the growth of columnar trunks.
- e) Volume-averaged concentrations for each phases (c_ℓ, c_c) are solved by global species conservation equations. To evaluate macrosegregation, a mixture concentration is defined: $c_{\text{mix}} = (c_\ell \rho_\ell f_\ell + c_c \rho_c f) / (\rho_\ell f_\ell + \rho_c f_c)$.
- f) A linearized binary Sn-Pb phase diagram with a constant solute redistribution coefficient k and a constant liquidus slope m is used.
- g) Interdendritic flow resistance in the mushy zone is calculated via a permeability law according to the Blake-Kozeny [14]. Solidification shrinkage is not accounted for and thermos-solutal convection is modelled with the Boussinesq approach.

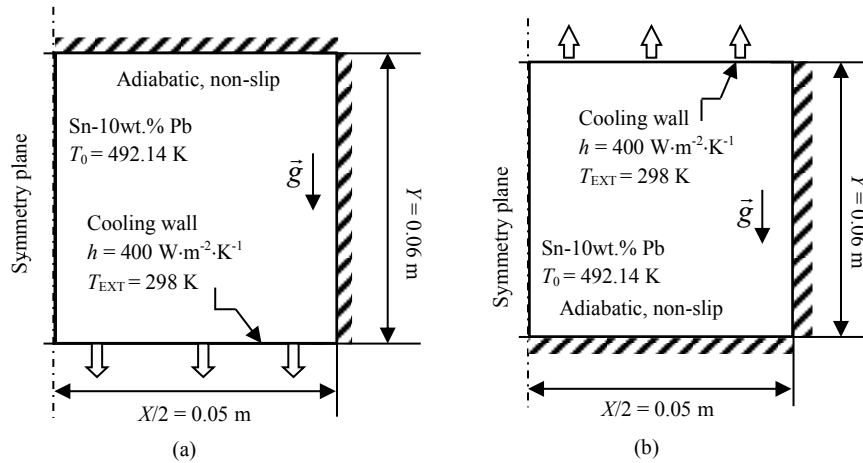


Figure 1. Benchmark geometry with boundary and initial conditions.

In this paper, a ‘macrosegregation index’,

$$c^{\text{index}} = \frac{c_{\text{mix}} - c_0}{c_0} \times 100 \quad (1)$$

and a ‘‘global macrosegregation intensity (GMI)’’ following reference [15],

$$\text{GMI} = \frac{1}{V_{\text{domain}}} \cdot \iiint_{V_{\text{domain}}} |c^{\text{index}}| dV \quad (2)$$

are used to qualify the macrosegregation and global severity of macrosegregation.

The benchmark simulations are carried out in 2D as shown in Figure 1, which is derived from the one proposed by Bellet et al [16], labelled with boundary and initial conditions. Due to the symmetry, half of the benchmark is modelled and a panel symmetry boundary condition is defined at the left boundary. In order to investigate the influence of the direction of gravity, the heat is extracted on the wall bottom (Figure 1(a)) or top (Figure 1(b)). In order to study the effects of different thermo-solutal

parameter on the melt convection and final macrosegregation, Sn-10wt. %Pb alloys is chose. Sn-Pb alloy system is a typical eutectic system and it has been investigated for a long time [17-19]. Furthermore, the thermal dynamic and physical properties are ready to obtain, and they can be found in references [17, 21-23].

There are two cases. Case 1, let the benchmark grow upwards from the bottom. Because the density of lead is much higher than tin, the solute enriched melt is heavier and have the tendency to flow downward. Case 2, let the benchmark grow downwards from top. The important features in the solidification process, such as growing direction, expand coefficient, flow convection, et al, can be investigated from the 2 benchmark cases.

Columnar solidification model is realized numerically with a control-volume based finite volume method through ANSYS FLUENT software version 14.5. Both the liquid and solid share a single pressure field P. The pressure correction equation is obtained from the sum of the normalized mass continuity equations using an extended SIMPLE algorithm [20]. For each time step, 60 iterations are adopted to decrease the normalized residual of concentration, flow quantities and pressure below 10^{-4} and enthalpy quantities below 10^{-7} . The time steps used impact the accuracy and reliability of the numerical results. Due to the complexity of the coupling, there is no formulation to determine the optimal Δt . It must be determined empirically by testing simulations. Initial time step 10^{-3} s is set. The iterations are run to the end of solidification at about 500 s and each simulation would take 2 days or so to complete the simulation on the parallel EVA cluster (2.6 GHz, 8 cores).

3. Simulation results

3.1 Case 1

This case considers the solidification of Sn-10wt.%Pb alloy from the bottom. The start of cooling immediately establishes a relatively stable temperature gradient. As soon as the temperature drops below the liquidus, the melt is undercooled, and solidification ($M_{lc} > 0$) begins Figure 2 (a.1). Since gravity force due to both thermal and solutal expansion points downwards, theoretically no flow should occur. Probably due to the numerical reason (inaccuracy or instability), a weak flow with the velocity magnitude of 10^{-6} m/s (Figure 2(c.1)) is induced. This weak flow leads to a weak segregation, $c^{\text{index}} \sim 0.28$. A relatively strong negative segregation at the bottom is obtained. This is due to diffusion of the solute in the interdendritic melt. It is known that segregation is originated from solute partitioning at the solidification interface. Given a control volume is isolated from its neighboring volume, there is no convectonal and diffusional mass exchange, and the solute partitioning can only cause microsegregation. Thus no macrosegregation would occur under this hypocritical condition. Here diffusional mass exchange is present as well. Therefore, there is mass exchange among neighboring control volumes through diffusion. Pb element is rejected into the interdendritic melt at the solid-liquid interface, causing a concentration gradient in the interdendritic melt. Diffusion in the interdendritic melt leads to formation of the negative segregation in the casting surface at the bottom at the initial solidification stage (Figure 2(d.1)). This negative segregation is slightly strengthened during the rest solidification (Figure 2(d.2), (d.3)). The top positive segregation layer forms in the same mechanism, i.e. diffusion of solute element in the interdendritic melt. In the end of the solidification, the columnar phase fraction has a very narrow range from 0.75 to 0.78, indicating that the solidification is a very steady one. The velocity during the solidification process is relatively small (at the magnitude of 10^{-3} m/s), and the final macrosegregation change for Case 1 is about -2.3 ~0.87.

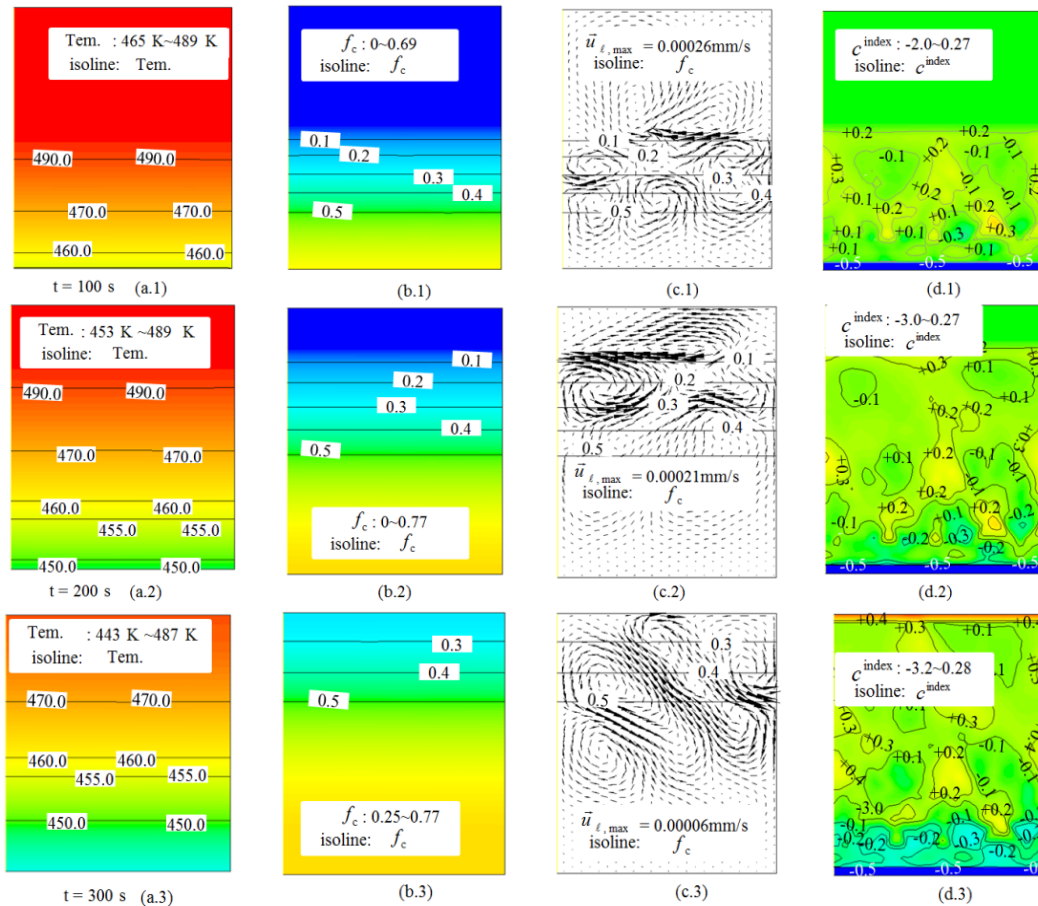


Figure 2. Simulation results of columnar solidification for Case 1: (a.1-a.3) evolution of temperature; (b.1-b.3) columnar phase fraction; (c.1-c.3) liquid velocity; (d.1-d.3) macrosegregation index. All of the qualities are shown in the color scales in addition to some isolines, with blue for the minimum (or negative extreme), and red for the maximum.

3.2 Case 2

Growing direction opposite, Case 2 solidifies with the heat extraction from the top. It can produce some unstable flow and generate strong convection during the solidification process. At the beginning, the temperature decreases (Figure 3(a.1)) and the melt affected by double influences of the thermal and solutal expansions starts to move downwards. A strong convection forms instantly after the mass transfer begins and the convection becomes more intensively as the phase transfer continues (Figure 3(c.1) and (c.2)). The convections in the melt varied acutely and decompose to more convection cells (vortex), taking on the feature of typical unstable flow and occupying the whole bulk liquid region. Since the permeability effect exists between liquid and columnar phase in the mushy zone, those connections are confined and driven to those area with the liquid fraction more than 0.7, which is shown in Figure 3(c.3). As a result, the velocity in the remained areas decreases to 10^{-4} m/s or less, which is ignorable and have no significant influence on the other scalars, such as temperature, species, pressure, et al. the phase fraction evolve gradually from 0 to 0.90 up to 300 s (Figure 3(b.1) - (d.2)).

Accordingly, the variations of macrosegregation are shown in Figure 3(d.1), (d.2) and (d.3). When the solidification starts, as is shown in Figure 3(d.1), channels form in top region adjacent to the chill

wall due to the unstable flow, but they are not well pronounced. This macrosegregation is in accordance with the weak flow pattern at the beginning. When the solid-liquid interface moves downwards, some channel segregation become significant. The liquid region has relatively homogenous species distribution without any stratification due to mixing effect of strong convections (Figure 3(d.2) and (d.3)), which stem from the instability of melt flow. The content of Pb becomes larger in the liquid phase as the solidification proceeds. As a consequence a severe positive macrosegregation region ($c^{\text{index}} \sim 124$) remains in the bottom when the solidification is completed. When the solidification time exceed about 400 s, the velocity in the whole domain decrease to 10^{-4} m/s or less, which is ignorable and have no significant influence on the other scalars, such as temperature, species, pressure, et al. The final GMI is about 39 and the global macrosegregation fluctuation in Case 2 would range from -58.2 to 156.0. The columnar phase distribution is also not homogeneous, ranging from 0.13 to 0.91. The rest melt solidifies as eutectic.

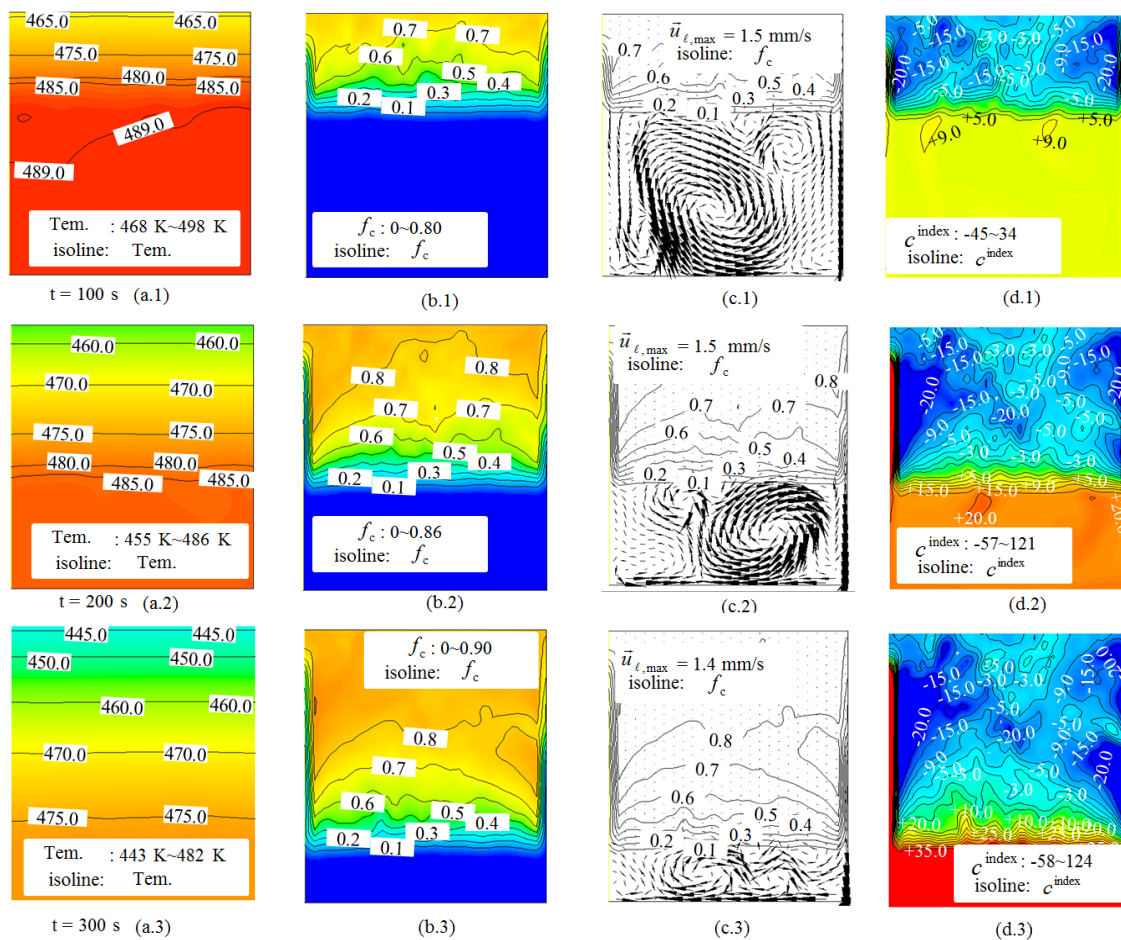


Figure 3. Simulation results of columnar solidification for Case 2: (a.1 - a.3) evolution of temperature contour; (b.1 - b.3) columnar phase fraction; (c.1 - c.3) liquid velocity; (d.1 - d.3) macrosegregation index. All of the qualities are shown in the color scales in addition to some isolines, with blue for the minimum (or negative extreme), and red for the maximum.

4. Discussion

4.1 Segregation by diffusion

In order to understand the formation mechanism of macrosegregation in detail, here two additional simulations are conducted. Both simulations are based on Case 1. For the simulation 1, the liquid

diffusion coefficient is set to a mini value $D_\ell = 1.0 \times 10^{-20} \text{m}^2 \cdot \text{s}^{-1}$ instead of its physical value of $D_\ell = 4.5 \times 10^{-9} \text{m}^2 \cdot \text{s}^{-1}$ to mimic the case without liquid diffusion, and no melt flow is included, i.e. the Navier-Stocks equation is ‘switched off’. The simulation result of macrosegregation is presented in Figure 4(a). Since there is no flow and diffusion is also ignored, the mixture concentration c_{mix} does not change at all over the calculation domain, staying at the value of the initial condition. For the simulation 2, the liquid diffusion is introduced ($D_\ell = 4.5 \times 10^{-9} \text{m}^2 \cdot \text{s}^{-1}$) while the other condition (no flow) is the same as the last simulation. The macrosegregation contour has obviously stratified, which is shown in Figure 4(b). Pb element is rejected into the interdendritic melt at the solid-liquid interface due to the solute partitioning ($k < 1$), causing a concentration gradient in the interdendritic melt. Diffusion in the interdendritic melt leads to formation of the negative segregation in the casting surface at the bottom at the initial solidification stage. Obviously, this kind of macrosegregation is dominated by liquid diffusion. This process is very stable and smooth, resulting in a gradually change of solute concentration over the benchmark, with a negative segregation layer in the bottom and a positive segregation layer in the top. The macrosegregation index range is very narrow, only from -0.7% to 0.6%. Here we can conclude that if there is no liquid flow, or the liquid is merely with ignorable velocity, the final macrosegregation is not significant.

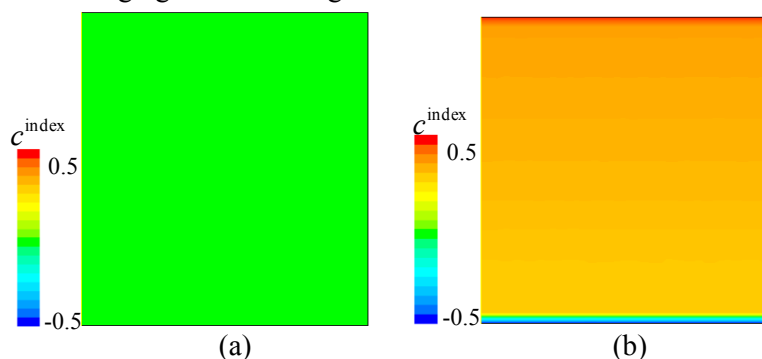


Figure 4. Final macrosegregation contours of two more simulations (calculations) based on Case 1: (a) Simulation 1: no flow is calculated and solute diffusion in liquid is ignored ($D_\ell = 1.0 \times 10^{-20} \text{m}^2 \cdot \text{s}^{-1}$); (b) Simulation 2: no flow is calculated, but solute diffusion in liquid is included ($D_\ell = 4.5 \times 10^{-9} \text{m}^2 \cdot \text{s}^{-1}$).

4.2 Segregation by thermo-solutal convection

Melt flow is not only sensitive to the thermal physical parameters, such as, thermal expansion coefficient, but also varied remarkably with solidification direction. For Case 2 the dominant factor for thermal solutal convection is the solutal expansion coefficient. For the Case 2, on the one hand, the solutal element Pb has significant potential to drive the liquid in the mushy zone move downwards. On the other hand, the solidification is from top to bottom, the ‘heavy liquid’ has sufficient space to move, thus presents the unstable flow in mushy zone, to generate different type of convections at different locations in the mushy zone. The interaction between those circulations can initiate some channel segregation.

The interdendritic melt, enriched with Pb, has a higher density than the bulk melt, and both the thermal and solute buoyancy forces lead to a downward flow in the solidification front, resulting in the global obvious convection in liquid region, which is indicated by white arrow in Figure 5(a). The magnitude of the velocity in the convection can reach $2.2 \times 10^{-2} \text{m/s}$. Despite the channels are originated from the unstable convention, complex convections are not all-sufficient conditions for the further growth, which needs some sensible species distribution in the liquid phase. Combining the species conservation equation and the mass conservation equation, and further considering the character of Pb-Sn phase diagram, the follow equitation can be derived:

$$\frac{\partial(c_\ell^* - c_\ell)}{\partial t} = (1-k) \frac{c_\ell}{f_\ell} \frac{\partial f_\ell}{\partial t} + \frac{1}{m} \frac{\partial T}{\partial t} + \vec{u}_\ell \cdot \nabla c_\ell \quad (3)$$

The third RHS term in Equation 3, $\vec{u}_\ell \cdot \nabla c_\ell$, is the so called flow-solidification interaction term, which is the most critical for growing of the channels. In according to different interdendritic flow, the sign of this term can be positive or negative. Local solidification behavior depends closely on the sign of the flow solidification interaction term. In a region where the velocity direction is same as the liquid concentration gradient, flow-solidification interaction term is positive, vice versa.

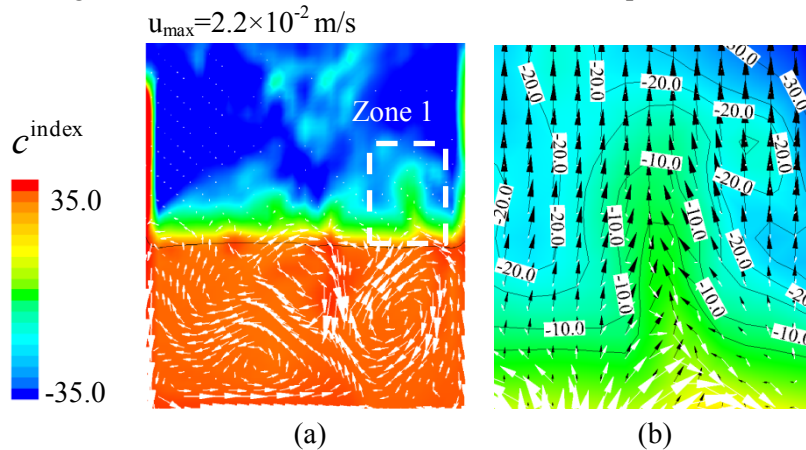


Figure 5. Simulation result for Case 2 at $t = 50$ s: (a) macrosegregation overlaid by liquid velocity vectors (white); (b) macrosegregation of Zone 1 in (a) overlaid by liquid velocity vectors (white) and gradient of liquid solutal concentration (black).

Channel segregation can form in the mushy zone, which is shown in Zone 1 in Figure 5(a). An enlarged Zone 1 is presented in Figure 5(b). The white arrow indicates the flow direction of liquid, while the black one is the direction of liquid concentration gradient. It can be clearly seen that in the channel, which has higher Pb concentration comparing to the neighboring parts, the direction of liquid velocity and liquid concentration gradient are opposite, resulting in a negative flow-solidification interaction term and retarding the solidification. On the contrary, the above-mentioned two directions are same for the areas on both side of the channel; it means that in those parts of the benchmark solidification is accelerated.

4.3 Macro-segregation and velocity magnitude

Some important solidification results are summarized in Table 2 for the above-mentioned four solidification benchmark cases. The distribution of liquid fraction, cooperating the interaction of thermal and solutal convection, gives the possibility to the evolution of velocity during the solidification of benchmark. Moreover, from the investigation in the previous sections the result can be concluded that those cases with large velocity differences have the ability to bear severer macrosegregation. When the flow is not included, the benchmark has homogeneous solutal distribution as initial value. As the velocity magnitude increases, up to range of $10^{-5} \sim 10^{-3} m/s$, the final macrosegregation index is controlled by diffusion mechanism, resulting in mild species fluctuation (ca. 3%). Case 1 is one of the examples. However, when the velocity of the cases, such as Case 2, reached the magnitude about $10^{-2} m/s$, the dominant factor for macrosegregation transfers from diffusion to thermal-solutal flow, and it can result in about 150% of macrosegregation index fluctuation over the domain.

Table 2. Statistic of solidification results for the liquid-columnar solidification benchmark.

Cases	Solidification time (s)	GMI at 600s (%)	Segregation range at 600s (%)	Range of f_c at 600 s (%)	Range of liquid velocity during solidification (m/s)
Case 1	465	0.038	-3.05~0.64	75.1~77.2	$0.0\sim 3.0\times 10^{-5}$
Case 2	465	38.22	-58.2~156	13~91.3	$0.0\sim 3.0\times 10^{-2}$
Case 1 without D_i	465	0.021	-0.13~0.3	75.2~76.3	$0.0\sim 1.0\times 10^{-5}$
Case 1 without flow	465	0.0	0.0	75.3~76.3	0.0~0.0

5. Summary

(1) For columnar solidification, thermal expansion and solute expansion coefficients of the melt are the key factors for the melt flow. The thermo-solutal convections and macrosegregation distribution are strongly influenced by the solidification direction.

(2) For columnar solidification model, macrosegregation is relative to convections velocity magnitude. For cases with flow convections velocity less than 10^{-3} m/s, the dominant factor for macrosegregation is the element diffusion in the interdendritic melt. The induced macrosegregation index fluctuation is about 3.0.

(3) When convections velocity is about 10^{-2} m/s, the dominant factor for macrosegregation is thermo-solutal convection, and it can result in about 150.0 fluctuation of c^{index} over the domain.

(4) Present study explored the effect of thermo-solutal convection on macrosegregation. It can give a comprehensive understanding to the mechanism of macrosegregation.

Acknowledgements

The authors acknowledge the financial support from Austrian Research Promotion Agency (FFG) through the project of Bridge Early Stage (No. 842441), as well as the technical support from the industrial partner Primetals Technologies (former Siemens VAI).

Reference

- [1] Beckermann C 2002 *Int. Mater. Rev.* **47** 243
- [2] Flemings M C 2000 *ISIJ Int.* **40** 833
- [3] Flemings M C and Nereo G E 1967 *Trans. Metall. Soc. Aime* **239** 1449
- [4] Dantzig J A and Rappaz M. EPFL Press, 2009
- [5] Li J, Wu M, Ludwig A and Kharicha A 2014 *Int. J. Heat Mass. Tran* **72** 668
- [6] Wu M, Domitner J and Ludwig A 2012 *Metall. Mater. Trans. A* **43** 945
- [7] Hachani L, Zaidat K and Fautrelle Y 2015 *Int. J. Heat Mass. Tran* **85** 438
- [8] Ahmad N, Rappaz J, Rappaz M and Combeau H 1998 *Metall. Mater. Trans. A* **29** 617
- [9] Li J, Wu M, Hao J and Ludwig A 2012 *Comp. Mater. Sci.* **55** 407
- [10] Li J, Wu M, Hao J, Kharicha A and Ludwig A 2012 *Comp. Mater. Sci.* **55** 419
- [11] Wu M, Li J, Ludwig A and Kharicha A 2013 *Comp. Mater. Sci.* **79** 830
- [12] Ludwig A and Wu M 2005 *Mater. Sci. Eng. A* **413** 109
- [13] Wu M and Ludwig A 2006 *Metall. Mater. Trans. A* **37** 1613
- [14] Poirier D 1987 *Metall. Mater. Trans. B* **18** 245
- [15] Wu M, Li J, Ludwig A and Kharicha A 2014 *Comp. Mater. Sci.* **92** 267
- [16] Bellet M, Combeau H, Fautrelle Y, Gobin D, Rady M, Arquis E, Budenkova O, Dussoubs B, Duterrail Y and Kumar A 2009 *Int. J. Therm. Sci.* **48** 2013
- [17] Bergman M I, Fearn D R, Bloxham J and Shannon M C 1997 *Metall. Mater. Trans. A* **28** 859
- [18] Sarazin J and Hellawell A 1988 *Metall. Mater. Trans. A* **19** 1861
- [19] Hebditch D and Hunt J 1974 *Metall. Mater. Trans.* **5** 1557
- [20] Patankar S V. Hemisphere Pub. Corp., 1980